


Article

Design and Comparative Analysis of an Ultra-Highly Efficient, Compact Half-Bridge LLC Resonant GaN Converter for Low-Power Applications

Muhammad Faizan ¹, Xiaolei Wang ^{1,2,*} and Muhammad Zain Yousaf ³ ¹ Institute of Microelectronics, Chinese Academy of Sciences, Beijing 100029, China; muhammad@ime.ac.cn² School of Microelectronics, University of Chinese Academy of Sciences, Beijing 100049, China³ School of Electrical and Information Engineering, Hubei University of Automotive Technology, Shiyan 442002, China; mzainy1@gmail.com

* Correspondence: wangxiaolei@ime.ac.cn

Abstract: For low-power applications, this paper presents the development and design of a compact and ultra-highly efficient half-bridge LLC resonant converter. By using Gallium Nitride (GaN) devices and high-efficient magnetics, the efficiency and power density of resonant converters can be improved. Compared to Silicon MOSFETs, GaN high-electron-mobility transistors (GaN HEMT) have a lower output capacitance and gate charge, resulting in lower driving loss and shorter dead times. Consequently, the proposed LLC converter based on GaN devices has excellent performance characteristics such as ultra-high efficiency, low switching losses, compact size, high voltage endurance, high operating temperature and high operating frequency. Furthermore, the proposed resonant converter features soft switching properties that ensure that the switches and diodes on the primary side are always switched at zero voltage and current. By doing so, LLC resonant converter switching losses are significantly reduced by up to 3.1%, and an overall efficiency of 98.5% is achieved. The LLC resonant converter design with GaN HEMT has great advantages over Si MOSFET solution regarding efficiency, overall losses, switching losses and power factor correction. A 240 W, 240 V to 60 V half-bridge GaN HEMT LLC resonant converter is simulated with a switching frequency of 75 KHz, along with the comparative analysis of the Si metal oxide semiconductor field effect transistor (MOSFET) solution. Moreover, the design and analysis of highly efficient magnetics with a power factor of 0.99 at full load is presented. A 240-Watt single stage LED driver with power factor correction is also designed to verify and compare the performance of proposed LLC resonant converter.

Keywords: LLC resonant converter; magnetics; wide band gap devices; high efficiency; power factor correction; zero voltage switching; LED driver



Citation: Faizan, M.; Wang, X.; Yousaf, M.Z. Design and Comparative Analysis of an Ultra-Highly Efficient, Compact Half-Bridge LLC Resonant GaN Converter for Low-Power Applications. *Electronics* **2023**, *12*, 2850. <https://doi.org/10.3390/electronics12132850>

Academic Editors: Arshad Arshad and Mohd Tariq

Received: 29 May 2023

Revised: 18 June 2023

Accepted: 21 June 2023

Published: 28 June 2023



Copyright: © 2023 by the authors. Licensee MDPI, Basel, Switzerland. This article is an open access article distributed under the terms and conditions of the Creative Commons Attribution (CC BY) license (<https://creativecommons.org/licenses/by/4.0/>).

1. Introduction

Since Dawon Kahng at Bell Laboratories created the first MOSFET in 1960, silicon-based MOSFETs have been employed as power devices [1]. Germanium (Ge) was utilized to create solid-state devices in the 1950s, but due to the small band gap (0.6 eV), these devices could only work at temperatures under 100 °C due to large leakage current at high temperatures [2]. As a result of silicon's 1.12 eV band gap and 1500 cm²/Vs electron mobility, devices can function at 200 °C [3]. Si has been the material of choice for the bulk of power devices for nearly five decades. The energy gap, electron mobility, thermal conductivity and electric field of Si as a material may become a restraining parameter in the near future. Incomplete body diode reverse recovery is another major issue with Si and SiC MOSFETs. The power MOSFET's partial body diode reverse recovery for the LLC resonant converter topology presents a possible system reliability concern [4]. Super junction technology in Si devices has nullified these restrictions to some extent [5,6].

Wide-bandgap (WBG) devices, such as SiC MOSFETs and GaN HEMTs, have recently attracted a lot of interest in the design of power electronics systems [7]. Wide-bandgap (WBG) devices have far quicker turn-on/off times, almost nil reverse recovery loss and significantly lower conduction losses than typical Si MOSFETs or insulated-gate bipolar transistors (IGBTs) [8]. In comparison to silicon, GaN has a substantially larger $1000 \text{ cm}^2/\text{Vs}$ electron mobility and band gap of 3.4 eV [9]. Due to the lack of an inherent body diode, GaN devices are better suited for use in high-frequency applications. In comparison to Si MOSFET, they also demand less drive power, which lowers drive losses. Higher-frequency operation enables highly efficient and more compact converters by lowering the size of resonant converter passive components, or in other words, by minimizing the size of magnetics [10]. Devices made of GaN also have a very small on-resistance for a specific breakdown voltage than Si devices. The device's on-resistance ($R_{(ON)}$) has inverse relation to both the third power of the energy gap E_G and the electron mobility (μ) [11,12].

$$R_{(ON)} \propto \frac{1}{\mu E_G^3} \quad (1)$$

For a given breakdown voltage, the on-resistance of a GaN HEMT will be nearly 15 times lower than that of a Si MOSFET. As a result, the converter's efficiency will increase by lowering conduction losses in the switches. On the other hand, GaN HEMTs have substantially lower output capacitance (C_{oss}) and gate charge (Q_g) than silicon MOSFETs, which leads to quicker on/off times and lower driving loss [13].

The switch-mode power supply was designed to operate at higher frequencies due to the recent need for high energy density, which is an unavoidable trend in the development of power electronics [14]. High-frequency, however, also entails high electromagnetic interference (EMI) pollution and high switching energy consumption [15,16]. Therefore, in the most recent few years, researchers from all over the world have been interested in resonant converters due to their soft-switching operation and high-frequency characteristic [17]. These converters are widely used in LCD TV power supplies, LED lighting drivers, EV charging stations, photovoltaic systems and for other useful products due to their advantages of high energy density and efficiency, magnetic integration, electrical isolation, low harmonic pollution and electromagnetic interference, wide output ranges, and low voltage stress [18]. The LLC resonant converters has combined benefits of all others resonant converters, containing DC isolation, reliable no-load operation, low needs of current ripples of capacitor filter, advantages in the voltage regulation of resonant current, soft-switching range [19].

On the other hand, ZVS at main side of power switches and ZCS at secondary side of rectifier diodes are used to run the LLC resonant converters. Therefore, these converters can attain high efficiency and low switching losses. Since these converters are frequency-controlled converters, the load characteristics and switching frequency have a significant impact on their output voltage. However, the optimal design of the reactive components is unaffected by the variable frequency control [20]. The power flow in these resonant converters is adjusted by shifting the converter's switching frequency below or above resonant frequency of resonant tank. Switching of resonant converters at zero current or zero voltage is possible [21,22].

Single-stage resonant converters with PFC were presented in [23–25] to minimize the drawback of Si MOSFET. In [23,24], a power factor corrected (PFC) converter is proposed with the application of resonant converter topology, and then it is applied to an LED driver [25], resulting in power supplies with greater efficiency and reduced profile. However, the switches work at asymmetrical duty ratio in these articles, which compromises the best power factor performance and complicates the driving and control circuits by adding 3rd harmonics to input current. The viability of LLC resonant topology functioning as a power factor correction converter with 50 percent duty cycle switch operation has been demonstrated in [26]. The viability of the LLC topology functioning as a PFC converter with 50% duty cycle switch operation is demonstrated in [26]. The authors of [27] presented

an interleaved parallel LLC resonant converter. The circuit architecture is more complex and has a small operating frequency range. In [28], an LLC resonant converter with a three-bridge arm has been presented. It is a hybrid of two complete bridges with the addition of two auxiliary switches on the secondary side. The authors of [18] presented a low-voltage LLC resonant converter. The whole input range is split into two parts: a high input voltage range and a low input voltage range. However, there is yet no simple LLC resonant converter design that provides good power factor correction with high efficiency and high power density. Therefore, for resonant soft-switching topologies which are working at high frequency like the LLC resonant converter, GaN HEMTs demonstrate considerable benefits over silicon MOSFETs. GaN HEMTs are widely utilized in low power consumption applications such as light emitting diode (LED) drivers, flat-screen TVs and laptop adapters due to their high power density [29]. GaN switches have been employed in a variety of non-isolated converters, achieving efficiencies of more than 97% [30]. In summary, the promise of gallium nitride (GaN) in power electronic devices will undoubtedly result in a more efficient and compact power converter industry.

In this paper, we design an ultra-highly efficient 240 W GaN LLC resonant converter with an input voltage of 240 V and output of 48 V for low-power consumer applications, including LED drivers, flat-screen TVs, laptop adapters, and all-in-one PCs. A 240-Watt single stage LED driver with power factor correction is also designed to verify and compare the performance of the proposed LLC resonant converter. The proposed LED driver has two separate secondary windings of the transformer which allow for the attachment of two independent LED strings. Although GaN switches have the ability to switch at a much greater frequency, the switching frequency is chosen to be 75 kHz due to large switching losses at high switching frequencies and large power requirements. A comparative analysis of transistors is performed using an analytical technique. Parameters like dead time (t_{dead}), turn-off energy (E_{off}), time-related output effective capacitance ($Co(tr)$), Q_{gd} and turn-off time (t_{off}) and reverse recovery charge (Q_{rr}), etc., are taken into account for the selection of a transistor, which can affect an LLC converter's high-performance accomplishments. Furthermore, an in-depth analysis of magnetic design is also offered. The advantages of GaN HEMT power transistors over Si MOSFETs transistors for soft-switching LLC resonant converters are also highlighted. Moreover, a comparative analysis between the two solutions is also presented in this paper. This comparison will help power electronics engineers choose the best architecture and devices.

The design is described in six sections. Section 2 of this paper is the structure of proposed resonant converter. Section 3 is the gain analysis. Section 4 emphasizes the design considerations. Section 5 is the simulation results. Section 6 is the conclusion.

2. Structure of Proposed LLC Resonant Converter

In this section, we have presented the structure of the proposed LLC resonant converter. Figure 1 presents the proposed topology of the GaN half-bridge LLC resonant converter. The LLC resonant tank contains magnetizing inductor (L_m), resonant inductor (L_r), resonant capacitors (C_r) and a transformer. The designed transformer for the proposed LLC resonant converter has one primary and two separate similar secondary windings. C11 and C12 and D11 and D12 are two output capacitors and rectifier diodes for 1st secondary winding, respectively. C21 and C22 and D21 and D22 are two output capacitors and rectifier diodes for 2nd secondary winding, respectively. For the LLC resonant converter operating at the resonance point and in the below resonance zone, the primary side half-bridge switches S1 and S2 always safely turn on without incurring switching loss. Additionally, switching losses are decreased, and the efficiency of the system is increased by using ZVS to turn on both switches and ZCS to turn on and off secondary side diodes.

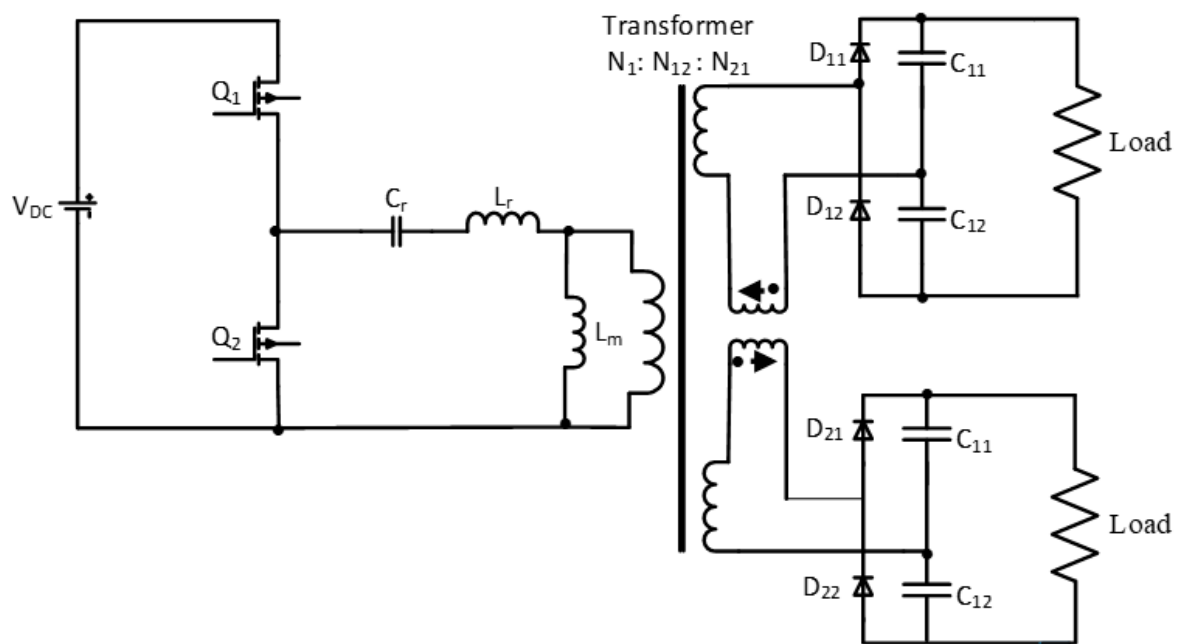


Figure 1. Proposed topology of half-bridge GaN LLC resonant converter.

A square wave is supplied into the half-bridge GaN HEMT-based LLC resonant converter, which outputs pure sinusoidal resonance frequency oscillations. The power is then supplied to the secondary windings of the transformer, where it is coupled to voltage doubler rectifiers, which turn the AC power into DC and supply it to the loads. The suggested system features two distinct secondary windings, allowing for the attachment of two independent LED strings to the transformer's secondary windings with an equal load. The mismatch effect between two identical windings is removed by the coupled inductor, which has no effect on power factor correction and efficiency of the LLC resonant converter. The suggested system features two distinct secondary windings, allowing for the attachment of two independent LED strings to the transformer's secondary windings with an equal load. A film capacitor system replaces the electrolytic capacitor system. Because the thin film capacitor has the advantages of higher temperature rating, stability of electrical values over long durations, low equivalent series resistance (ESR) for higher ripple current handling, higher surge voltage rating and self-healing. The component's life is even longer than the life period specified in the datasheet if the switch was used in typical working circumstances [31]. The magnetizing current I_{Lm} and the current secondary I_{Lr} multiplied by transformer turns ratio n make up the LLC's current of the primary I'_{Lr} . The magnetizing current must discharge the transformer's inter-winding and intra-winding capacitance and the transistors' parasitic output capacitance to accomplish zero voltage switching (ZVS) for transistor turn-on without any turn-on loss of switches. On the other hand, the parasitic output capacitance of the transistor was entirely drained by employing this magnetizing current during each dead period to accomplish the ZVS for turn-on. Therefore, the minimum magnetizing current is achieved to improve the efficiency of the proposed half-bridge LLC resonant converter.

Operational Principle of GaN LLC Resonant Converter

During time interval $0 - \frac{T}{2}$, magnetizing and load current passes through the switch Q1 and diodes D11 and D12. During this time interval, the real power flow occurs from the input to the output. Therefore, this phase is also referred to as the power transfer stage. See Figure 2.

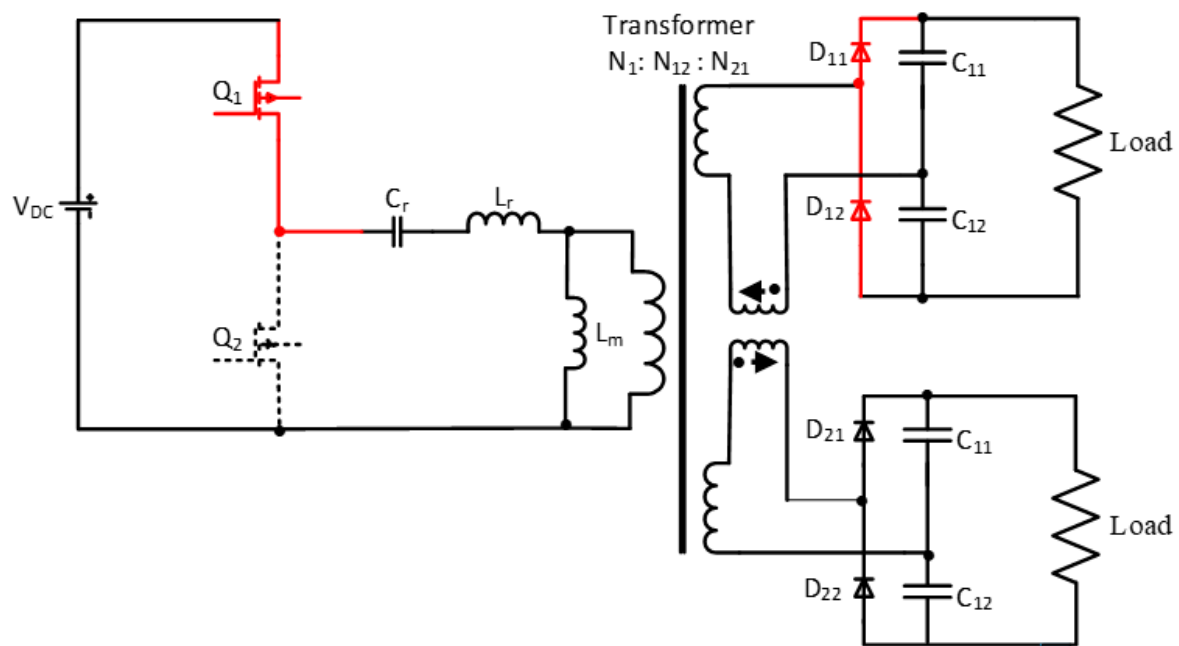


Figure 2. The general operation of LLC resonant converter for time interval $0 - \frac{T}{2}$.

During time interval $\frac{T}{2} - T$, magnetizing current along with load current passes through the switch Q2 and diodes D21 and D22. In addition, during this time interval, the real power flow occurs from the input to the output. Therefore, this phase is also referred to as the power transfer stage. See Figure 3.

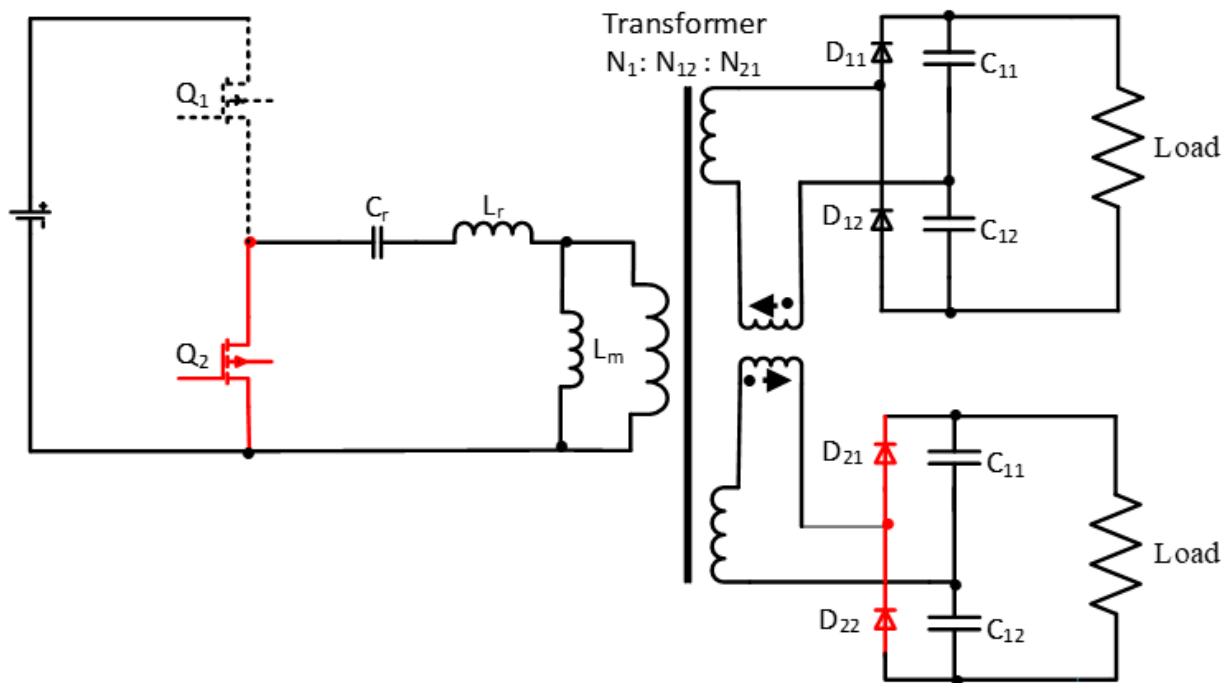


Figure 3. The general operation of LLC resonant converter for the time interval $\frac{T}{2} - T$.

Figure 4 describe operating circuits and waveforms for different quadrants, and also loss breakdown for steady-state cycle of the proposed half-bridge LLC resonant converter.

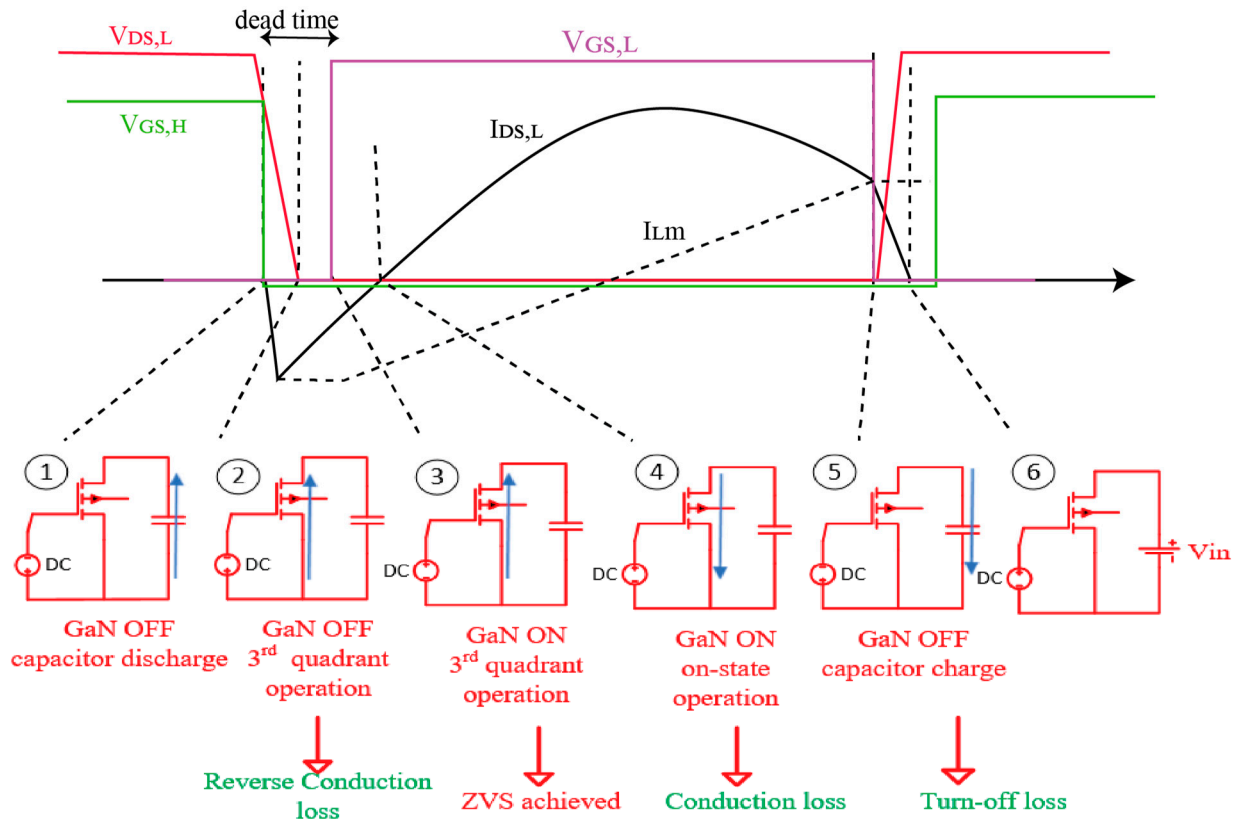


Figure 4. Operation and loss breakdown for steady-state cycle for the proposed half-bridge LLC resonant converter.

3. Gain Analysis of the Proposed Converter

In this section, the first harmonic approximation approach is used to investigate the gain characteristics of a half-bridge GaN HEMTs-based LLC resonant converter. Let “ ωs ” be the switching frequency and “ V_k^F ” be the resonant tank circuit’s fundamental input voltage component.

$$V_{bc}(\omega t = \theta) = V_{nk} \sin(\omega s t) \quad (2)$$

$$V_{nk} = \frac{2V_{bus}}{\pi}$$

$$V_{bc}(\omega t = \theta) = \frac{2V_{bus}}{\pi} \sin(\omega s t) \quad (3)$$

$n = 1$, for the fundamental component:

$$V_{bc(rms)}^F = \frac{2V_{bus}}{\sqrt{2}V_{bus}\pi} \sin(\omega s t) \quad (4)$$

$$V_{bc(rms)}^F = \frac{2V_{bus}}{\sqrt{2}\pi}$$

Transformer secondary current is determined by:

$$I_{s(rms)} = \frac{\sqrt{2}I_o\pi}{2} \quad (5)$$

The secondary voltages ($V_{S(rms)}^F$) of the transformer can be calculated as:

$$V_S^F(t) = \frac{4V}{\pi} \sin(\omega s t) \quad (6)$$

The transformer's secondary voltages are half as high as the output voltages due to the voltage doubler rectifier.

$$V_S^F(t) = \frac{2V_o}{\pi} \quad (7)$$

where V_o is the peak voltage.

Equation (7) is divided by $\sqrt{2}$ to find the RMS value of the transformer's secondary voltages:

$$V_{S(rms)}^F = \frac{2V_o}{\sqrt{2}\pi} \quad (8)$$

R_{ac} of voltage doubler rectifier can be determined as:

$$R_{AC} = \frac{V_{S(rms)}}{I_{S(rms)}} \quad (9)$$

$$R_{AC} = \frac{2R_o}{\pi^2}$$

For simplification of the analysis, the resistance of the secondary side has been referred to as the resistance of the primary side:

$$R_P = R_S n^2 \quad (10)$$

$$R_P = R'_{AC} = \frac{2R_o n^2}{\pi^2}$$

where R_P and R_S are the resistances of primary and secondary sides respectively.

Voltage across the R'_{AC} can be calculated by (11), which is similar to the transformer's primary side voltage:

$$V_{primary} = 2V_{s(rms)}^F \quad (11)$$

$$V_{primary} = V_{Lm} = \frac{2nV_o}{\sqrt{2}\pi}$$

DC gain "Gdc" and voltage gain 'M' of the GaN LLC resonant converter is calculated as follows:

$$V_{Lm} = \left| \frac{X_{Lm} \| R_{ac}'}{(X_{Lm} \| R_{ac}') + X_{Lr} + X_{Cr}} \right| \times V_{ab} \quad (12)$$

$$M = \frac{V_{Lm}}{V_{ab}} = \left| \frac{X_{Lm} \| R_{ac}'}{(X_{Lm} \| R_{ac}') + X_{Lr} + X_{Cr}} \right|$$

$$M = \frac{\frac{X_{Lm} \times R_{ac}'}{X_{Lm} + R_{ac}'}}{\frac{X_{Lm} \times R_{ac}'}{X_{Lm} + R_{ac}'} + [1 + (X_{Lr} + X_{Cr}) / \frac{X_{Lm} \times R_{ac}'}{X_{Lm} + R_{ac}'}]}$$

$$M = \frac{A}{\sqrt{\left[1 + A - \frac{1}{f_n^2}\right]^2 + Q^2 A^2 \left(f_n - \frac{1}{f_n}\right)^2}}$$

$$G_{dc} = \frac{1}{n} \times \frac{A}{\sqrt{\left[1 + A - \frac{1}{f_n^2}\right]^2 + Q^2 A^2 \left(f_n - \frac{1}{f_n}\right)^2}} \quad (13)$$

where "Q" is the quality factor,

$$A = \frac{\text{magnetizing inductance}}{\text{resonant inductance}}$$

where n is the transformer's turn ratio, f_r is resonance frequency and f_n normalized frequency. The Proposed converter's input power can be computed from Equation (14).

$$P_{input} = \frac{2}{T_s} \int_0^{\frac{T_s}{2}} I_{avg(in)} \times V_{in} dT \quad (14)$$

$$P_{input} = \frac{V_p^2}{16 \times L_b \times f_s} \left[\frac{1}{2} - \frac{2 \times V_p}{3 \times \pi \times V_{bus}} \right]$$

For the calculation of maximum gain, DC bus voltages should not be lower than the peak value of the input voltages. So, minimum and maximum gain can be determined from Equations (15) and (16):

$$M_{\text{minimum}} = 1 \quad (15)$$

$$M_{\text{maximum}} = \frac{nV_o}{V_{\text{bus}(\text{minimum})}} = \frac{9.9 \cdot 60}{240} = 2.475 \quad (16)$$

At the parallel resonance frequency $\frac{f_p}{f_r} = 0.392$, the proposed LLC resonant tank has a normalized gain of 2.71, which is 9% greater than the required gain of 2.5. If the LLC resonant converter gain will satisfy the PFC need at peak voltage, then it will fulfil the needs for the whole line voltage cycle. To assure zero voltage switching, the proposed GaN LLC converter is worked in an inductive region. Figure 5 shows the proposed resonant converter's typical voltage gain curve.

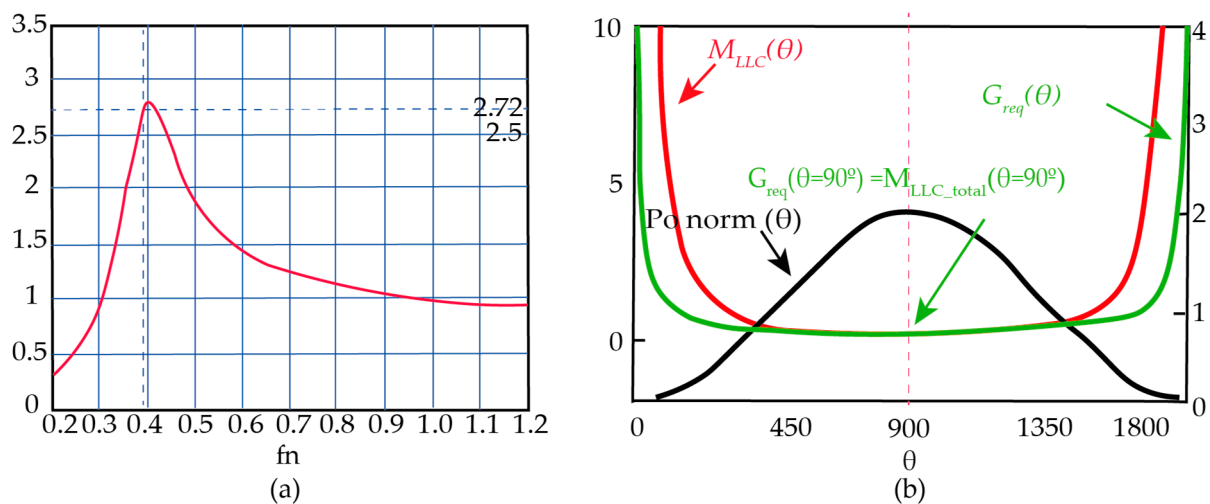


Figure 5. Designed LLC resonant converter gain plot (a) Normalized gain plot at the heaviest load. $P_o(\theta = 90^\circ) = 2P_o$ (b) Gain Requirement vs. gain curve $V_o = V_o^{\text{max}} = 60$ V.

Table 1 contains all the basic design specifications of LLC resonant converters.

Table 1. Basic design specifications.

Parameters	Values
V_{in}	200–240 V
V_{out}	60 V
P_o	240 W
Switching frequency (f_s)	75–250 KHz
I_o	4–10 A
f_r	100 kHz

4. Design Consideration

In this section, we present a detailed design of the transistor, transformer, capacitor, and inductor for half-bridge LLC resonant converter.

Primary Transistors Selection: The following are key parameters for the selection of transistor for LLC resonant converter.

Dead time (t_{dead}): The minimum dead time t_{deadmin} of half-bridge LLC resonant converter for ZVS achievement can be calculated as:

$$t_{\text{deadmin}} = 16 \cdot C_{o(tr)} \cdot L_m \cdot f_s \quad (17)$$

Here, $C_{o(tr)}$ is time-related effective output capacitance.

Time related effective output capacitance ($C_{o(tr)}$): For high-density and high-efficiency LLC converters, the transistor parameter $C_{o(tr)}$ defines the output capacitance required to transmit the voltage from the drain to the source passively. A shorter dead time and larger magnetizing inductance value for the transformer are made possible by a lower effective $C_{o(tr)}$, which also reduces circulating losses on the primary side for provided drain-to-source transition time. Meanwhile, for a given value of t_{dead} and L_m , the smaller value of $C_{o(tr)}$, the larger ' f_s ' can be utilized with ZVS condition to design a higher density LLC resonant converter.

This $C_{o(tr)}$ derived from ' Q_{oss} ' and Q_{oss} , which are related by the following equations:

$$Q_{oss} = \int_0^{V_{ds}} C_{oss}(v) dv \quad (18)$$

$$C_{o(tr)} = \frac{Q_{oss}}{V} \quad (19)$$

Figure 6 presents the plots between Q_{oss} and V_{ds} with V_{ds} transition from 240 V to 0 V, Si MOSFET has 10 times larger $C_{o(tr)}$ than GaN HEMT and SiC MOSFET has a 50% larger $C_{o(tr)}$ than GaN HEMT.

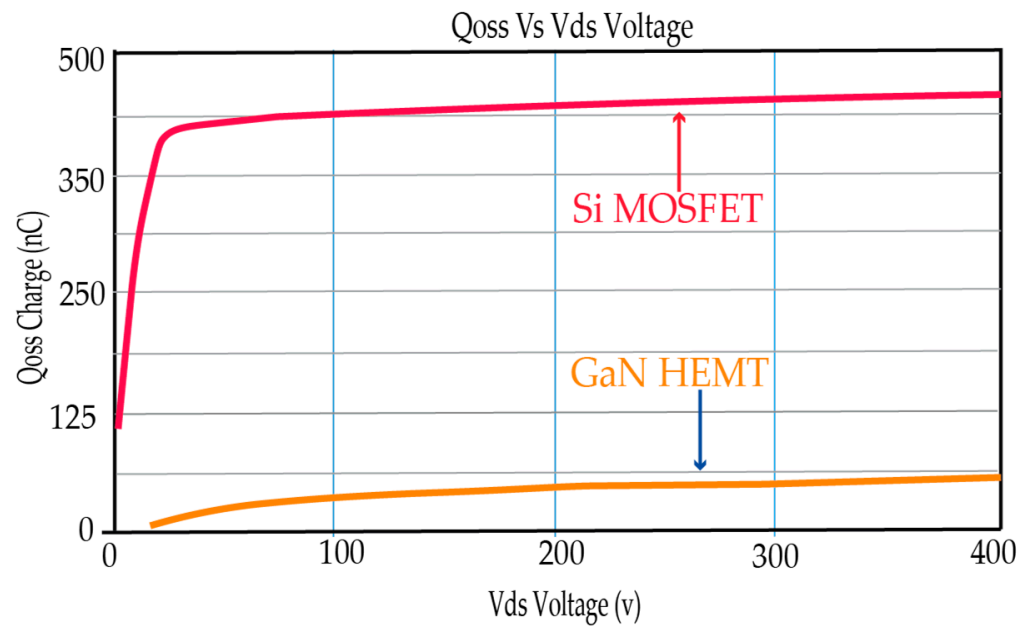


Figure 6. Q_{oss} vs. V_{ds} curves for GaN HEMT and Si MOSFET.

Q_{gd} and turn-off time (t_{off}): Q_{gd} , which defines the charge necessary for the gate to drain switching while the switching turn-off time (t_{off}) is another crucial transistor parameter for LLC resonant converter design. These two metrics indicate the efficiency and maximum operating frequency by indicating turn-off capabilities and losses. With the provided switching voltage and current circumstances, the turn-off time (t_{off}), which is often not listed in the transistor datasheet, can be approximated following the reference book [32].

Reverse recovery charge (Q_{rr}): The body diode's current reverse recovery charge (Q_{rr}) will produce high dv/dt and a significant shoot-through current that might cause a MOSFET breakdown in the bridging transistors. The lower the Q_{rr} value, it is better to avoid failure since it is a crucial parameter for determining the hazard for the hard commutation failure mode.

Transformer: The detailed design of a high-frequency transformer is presented in this section. For the achievement of maximum efficiency and compatibility with the designed circuit parameters, the transformer design is carried out. For the core of the transformer, we use power ferrite 3C95 material from Ferroxcube to lower core loss. GaN HEMTs allow the LLC Resonant Converters to operate at a high switching frequency (F_{sw}), as described above. The effective core area (A_e) and primary side winding turns (N) decrease as the switching frequency rises. With the reduction in core size, the power density increases. The correlation between switching frequency and core size is shown in the form of magnetic flux density (B) Equation (20).

$$\Delta B_{max} = \frac{0.5 \times N \times V_O}{N_p \times A_e \times F_{sw}} \quad (20)$$

Equation (21) gives the transformer leakage inductance:

$$\text{Leakage Inductance} = L_{LK} = \mu_0 \frac{N^2 l_w}{M^2 b w} \left[\frac{1}{3} \sum h p + \sum \Delta h \right] \quad (21)$$

where N is the number of turns, bw is the breadth of winding, l_w is the mean turn length, ' M ' is the number of primary–secondary intersections, Δh is the height of the primary–secondary intersection and hp is the height of pth winding portion.

By using the resistance factor F_R , transformer ac resistance winding can be calculated as

$$F_R = \frac{R_{ac}}{R_{dc}} = \varphi \frac{\sinh 2\varphi + \cosh 2\varphi}{\cosh 2\varphi - \cos 2\varphi} + \frac{2(m^2 - 1)}{3} \varphi \frac{\sinh \varphi - \sin \varphi}{\cosh \varphi + \cos \varphi} \quad (22)$$

where δ is the penetration depth, m is the number of winding layers, $\varphi = \frac{h}{\delta}$, h is the height of the conductor and R_{ac} and R_{dc} are the ac and dc winding resistance respectively.

Transformer inter-winding capacitance ' C ' can be determined as

$$C = \epsilon_0 \epsilon_r \frac{A}{d} \quad (23)$$

where ' A ' is the area of winding, ' ϵ_r ' is relative permittivity, ' ϵ_0 ' is the permittivity of free space, and ' d ' is the distance between windings.

Inductor: In order to lower the inductor's ac losses, two distinct windings (dc and ac windings) are used. Since thin ac windings have lower ac resistance, therefore they carry the majority of the ac ripple current. Similarly, thick dc windings have lower dc resistance; therefore, they carry the majority of the ad current. This will lower the inductor's winding losses. As a result, efficiency will improve. We used Magnetics Kool M μ core to minimize the core loss.

Equation (24) gives the value of the resonant inductor (L_r)

$$L_r = \frac{Q \times R_{ac}}{2\pi f_r} \quad (24)$$

Equation (25) gives the value of magnetizing inductor (L_m)

$$L_m = A \times L_r \quad (25)$$

The number of turns of the coupled inductor can be determined by Equation (26).

$$N_1 = \frac{V_{max}}{A_{core} \times w \times B_{core}} \quad (26)$$

Capacitors: Ceramic capacitors are chosen for the input and output sides of the LLC resonant converter to decrease the size of the Equivalent Series Resistance (ESR) and converter. The value of the resonant capacitor is determined as:

$$\text{Resonant capacitance} = C_r = \frac{1}{L_r \times (2\pi f_r)^2} \quad (27)$$

Comparative Analysis of GaN HEMT and Si MOSFET for LLC Resonant Converter

The most modern Si-based MOSFET with an inherent fast body diode was selected for comparative analysis. The most recent wide bandgap HEMTs are more suitable for high-density and high-efficiency power conversions. Table 2 demonstrates the advantages of GaN power transistors over Si for LLC resonant converter critical parameters. For the better performance of highly efficient and high power density LLC resonant converter designed, the values of $C_{o(tr)}$, Q_{gd} , t_{off} and Q_g should be low. The GaN HEMT has lower values for all these parameters as compared to Si MOSFET. A lateral two-dimensional electron gas channel generated on a GaN heterojunction with no inherent bipolar body diode is another important feature of GaN power transistors for the design of high-efficiency LLC resonant converter. Without body diode for GaN HEMT, Q_{rr} is zero, which prevents the hard avalanche behavior as described above due to the presence of body diode for Si MOSFET. GaN FETs are the majority carriers, unlike Si MOSFETs. Therefore, there is no reverse recovery charge, hence no reverse recovery losses. Three types of losses occur in power switches that are: (1) conduction losses (determined by $R_{DS(ON)}$) (2) driving losses (determined by Q_g), and (3) switching-off losses (determined by C_{oss}). We analyzed that the GS66508B has mentioned advantages for these losses reduction over the Si MOSFET IPx65R110CFD when working at higher frequency with soft-switching for half-bridge LLC resonant converter.

Table 2. Key transistor parameters comparison for LLC resonant converter.

Parameters	GS 66508B	IPx65R110CFD MOSFET	GaN's Value
	GaN	Si	
V_{ds} ; V	650	600	Typically same almost
$R_{DS(on)}$; mΩ	52	50	Typically same almost
$C_{o(tr)}$; pF	144	1173	The shorter dead time for LLC, very small circulating loss
Q_{gd} ; nC	1.7	28	Very small switching turn-off loss
t_{off} ; ns	2.53	15.2	Very small switching turn-off loss
Q_g ; nC	5.82	79.5	Lower gate drive and switching loss
Q_{rr} ; nC	0	719	No hard communication failure

5. Simulation Results

The designed LLC resonant driver has output voltages of 60 V, 240 W output power and is driven by a 240 V AC at 75 kHz frequency. A thorough simulation analysis of the design converter is carried out to improve the design. The LLC resonant converter model is simulated on CADENCE under different test conditions to verify performance and operation. Figure 7 shows the typical operational waveforms of the LLC resonant converter.

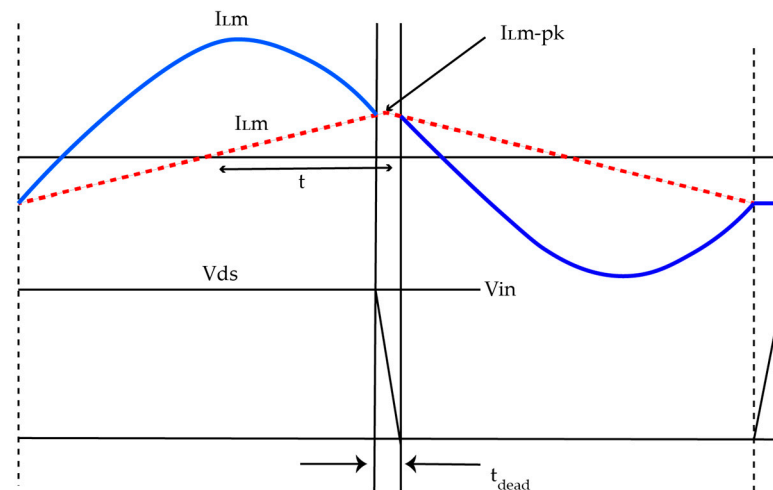


Figure 7. Primary voltage and current waveform for the proposed LLC resonant converter. The current and voltage are presented by blue and red lines, respectively, while the magnetizing and resonant current are shown by orange dotted lines and solid black lines respectively.

In Table 3, all the losses of different components of LLC resonant converter are mentioned.

Table 3. Calculated losses in different components of GaN LLC resonant converter.

Losses	Idle Losses	Conduction Losses
GaN Switches	0.017 W	3.3 W
Transformer	0.82	2.34 W
Inductor	0.43	1.27 W
Capacitor	-	0.15 W
Switching		2.25 W

The computed percentage loss distribution of the converter at full load is shown in Figure 8. Magnetic losses are responsible for about 40% of losses due to copper and core losses. Approximately 50% of the total losses are due to switch deriving and conduction losses.

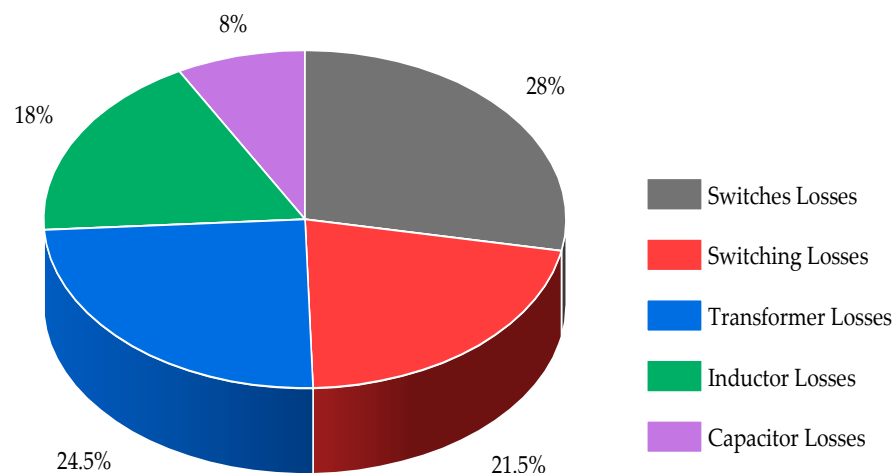


Figure 8. Percentage Loss distribution of the LLC resonant converter at full load.

It is clear from Figure 9 GaN HEMT has a great advantage in both switching performance and conduction for LLC resonant converter applications.

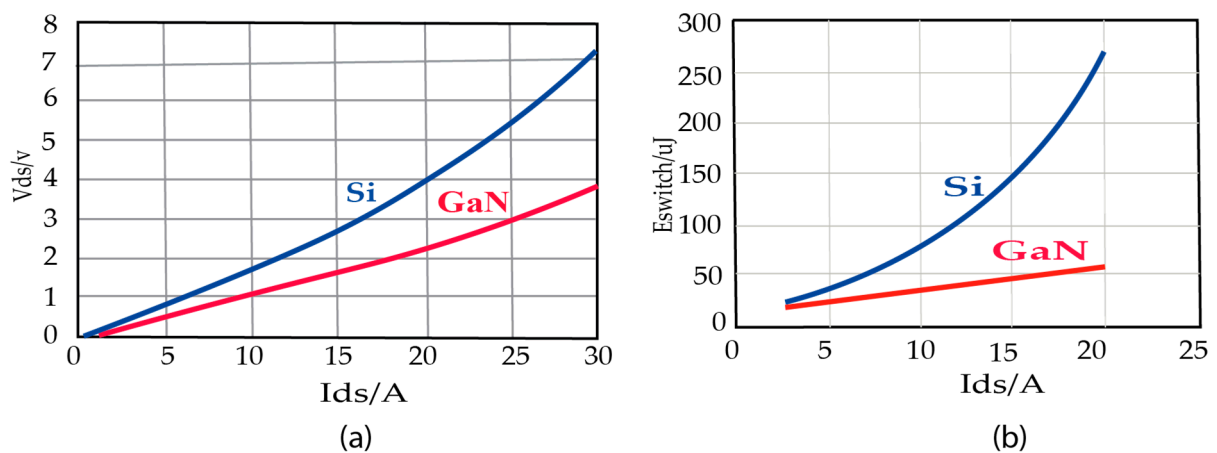


Figure 9. Switching loss Characteristics comparison among GaN HEMT, Si MOSFET for LLC resonant converter. (a) Drain Source voltage (V_{ds}) and drain source current (I_{ds}). (b) Switching loss and drain source current (I_{ds}).

Transformer primary terminal voltage and current, and rectifier output voltage is shown in Figure 10. The waveform of rectifier output voltage is perfect square wave.

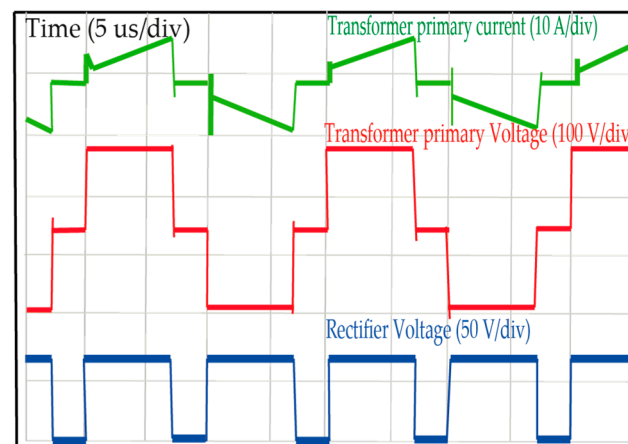


Figure 10. GaN based LLC resonant converter waveforms for transformer primary terminal voltage and current and rectifier output voltage.

Figure 11 shows the input current, voltage and output current. A 0.99 power factor is achieved.

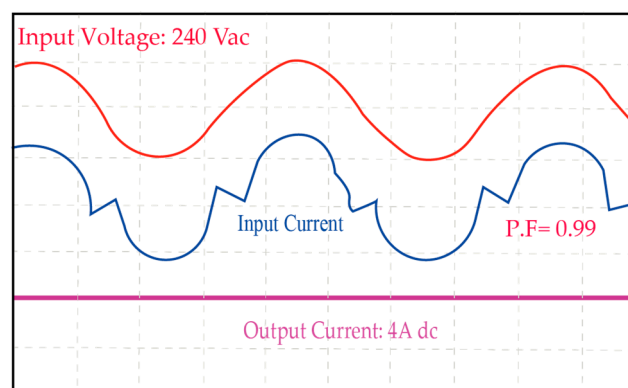


Figure 11. LLC resonant converter Power factor performance when $V_{in} = 240$ V, $I_{out} = 4$ A. $V_{out} = 60$ V.

Figure 12 shows that ZVS performance was achieved during the whole LLC resonant converter operation. This significantly lowers switching loss and increases the overall efficiency of the converter.

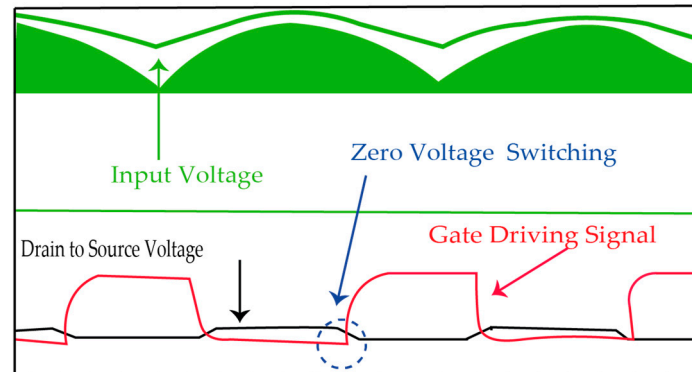


Figure 12. Zero voltage switching performance of LLC resonant converter operation.

The major loss differences come from the primary side transistors if the loss breakdown of other components, such as the inductor, capacitor and transformer, is expected to be the same. Even if the LLC converter achieves ZVS for turn-on, the switching turn-off loss persists with the magnetizing current on the main, especially at higher switching frequencies. Despite the fact that these turn-off losses cannot be ignored, GaN HEMTs have very low switching turn-off losses. In addition, the GaN-based LLC has very small drive losses. In short, the GaN-based LLC converter achieves excellent efficiency, and this increase in efficiency offers the incremental performance necessary for low-power applications to surpass the most recent industrial system requirements. Figure 13 shows maximum efficiency at rated voltage and current, i.e., 240 V and 4 A. Such a highly efficient proposed design gives a cost-effective solution compared to a Si MOSFET-based LLC resonant converter. The maximum efficiency achieved for the proposed LLC resonant converter is 98.5%.

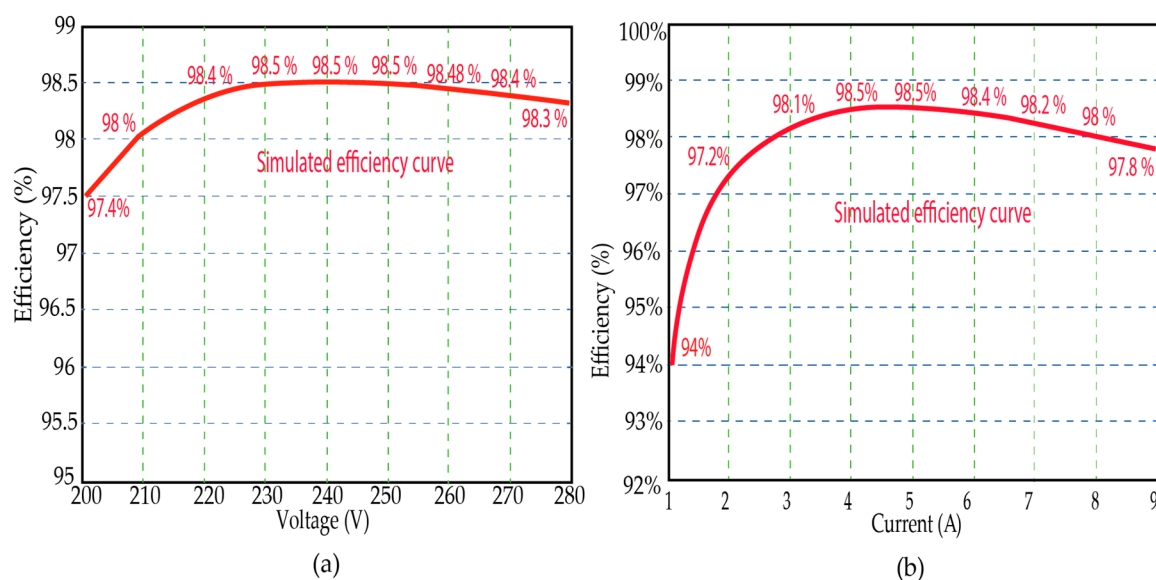


Figure 13. Efficiency curves of GaN based LLC resonant converter (a) The efficiency performance at different input voltage (b) The efficiency performance at different loads (1 A, 190 W to 9 A, 240 W).

Figure 14 shows the power factor comparison of the two solutions. It is clear from the figure that the GaN HEMT solution has a much better power factor than the Si MOSFET solution.

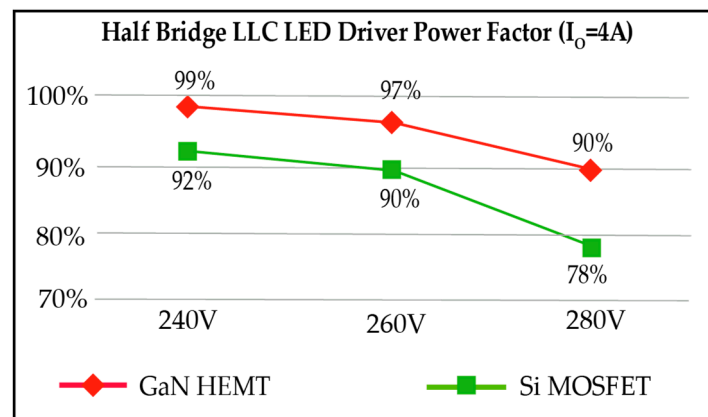


Figure 14. Power Factor performance comparison of the resonant converter with GaN HEMT and Si MOSFET.

Switching turn-off losses, which Si MOSFET has six times more than that of GaN HEMT, are the most significant losses for Si MOSFET-based LLC resonant converter compared to that of GaN HEMT. Additionally, the drive loss of the GaN LLC resonant converter is substantially lower than that of Si MOSFETs. Overall simulation results indicate that compared to Si, the GaN LLC resonant converter has around 37% fewer total losses. Figure 15 shows the efficiency comparison of the two solutions. In summary, GaN LLC resonant converter achieves excellent efficiency. This increase in efficiency gives the incremental performance necessary for low-power applications to surpass the most recent industrial system requirements.

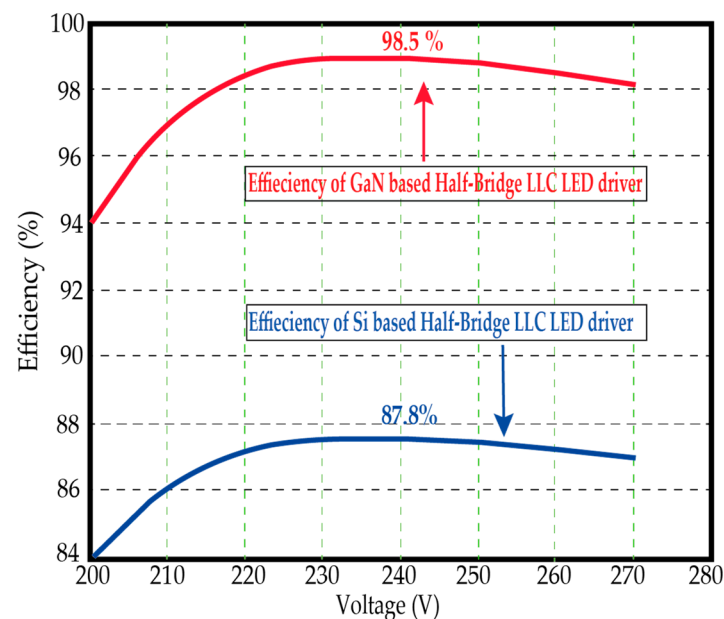


Figure 15. Efficiency comparison of designed LLC resonant converter with GaN HEMT and Si MOSFET.

Compared to GaN HEMT-based LLC resonant converter, the switching turn-off losses for Si MOSFET-based LLC resonant converter are the most significant losses. In addition, GaN HEMTs-based resonant converter has a much lower drive than that of Si MOSFETs.

Overall simulation results indicate that compared to Si MOSFETs solution, the GaN LLC resonant converter has around 37% fewer total losses. A loss comparison of two solutions for LLC Resonant Converter is shown in Figure 16, which shows that GaN HEMT has significant advantages on switching performance and conduction for LLC resonant converter design.

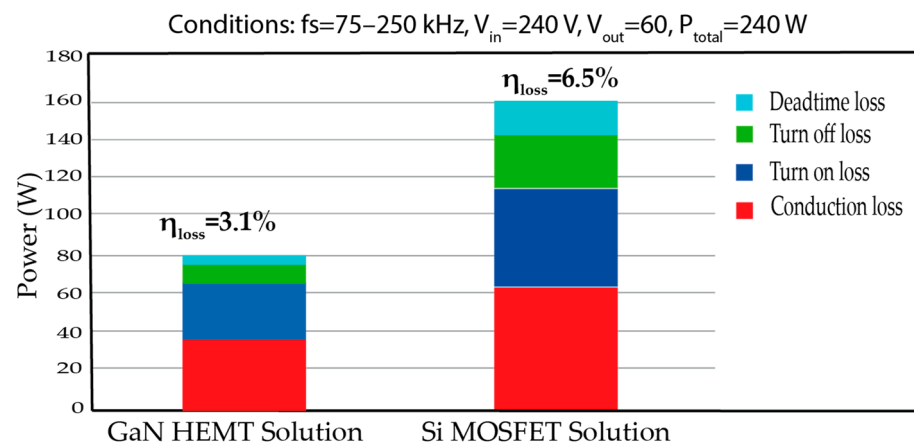


Figure 16. Loss comparison of two solutions for LLC Resonant Converter.

Table 4 shows that the LLC resonant converter design with GaN HEMT has great advantages over the Si MOSFET design.

Table 4. Performance comparison of LLC resonant converter with GaN HEMT and Si MOSFET.

Parameters	GaN HEMT	Si MOSFET
Power factor (P.F)	0.99	0.92
Efficiency	98.5	87.4
Total Losses	3.1%	6.5%
Switching losse	1.5	2.8

6. Conclusions

An ultra-high-efficient and very compact GaN LLC resonant converter with 240 W, 240 V and 75 kHz is presented in this paper for low power applications. A 240-Watt single stage LED driver with power factor correction is also designed to verify and compare the performance of the proposed LLC resonant converter. A comparative analysis regarding efficiency, power factor correction and losses is performed for LLC resonant converter design with GaN HEMTs and Si MOSFETs. Design and analysis of highly efficient magnetics (inductor and transformer) is also conducted. Simulation results show that the proposed GaN HEMTs-based resonant converter is more highly efficient and cost-effective than the Si MOSFETs based resonant converter. With GaN HEMTs, the LLC resonant converter has an efficiency of 98.5% with 0.99 PFC instead of 87.4% with 0.92 PFC in the case of Si MOSFETs. GaN HEMTs-based LLC converters have around 37% lower total losses than Si MOSFETs. Increasing efficiency provides the incremental performance for low-power applications to surpass the most recent industrial requirements. Comparative analysis and simulation results show that GaN HEMTs with lower Q_{gd} , $Co(tr)$, Q_g and t_{off} values are most suitable for the LLC resonant converter design from the standpoint of power density and efficiency. Furthermore, the GaN HEMT-based LLC resonant converter design is more reliable because the Q_{rr} is zero, and the body diode is also not present.

Author Contributions: Conceptualization, X.W., M.F. and M.Z.Y.; methodology, X.W., M.F. and M.Z.Y.; software, X.W., M.F. and M.Z.Y.; validation, X.W., M.F. and M.Z.Y.; mathematical analysis, X.W. and M.F.; investigation, M.Z.Y. and M.F.; resources, X.W., M.F. and M.Z.Y.; writing original draft preparation, X.W., M.Z.Y. and M.F.; writing review and editing, X.W., M.F. and M.Z.Y.; visualization, X.W.; supervision, X.W.; project administration, X.W. and M.F.; funding acquisition, X.W. All authors have read and agreed to the published version of the manuscript.

Funding: This work is supported by the National Key Research and Development Program of China (No. 2022YFB4400300). The APA was founded by Xiaolei Wang (corresponding author).

Data Availability Statement: Not applicable.

Acknowledgments: The authors are grateful to the School of Microelectronics, Chinese Academy of Sciences, Beijing-China, and the School of Electrical and Information Engineering, Hubei University of Automotive Technology Shiyan, China, for conducting this research.

Conflicts of Interest: The authors declare no conflict of interest.

References

1. Scott, R.S.; Franz, G.A.; Johnson, J.L. An accurate model for power DMOSFETs including interelectrode capacitances. *IEEE Trans. Power Electron.* **1991**, *6*, 192–198. [\[CrossRef\]](#)
2. Lu, J.L.; Qiu, Y.; Chen, D. A full power emulation platform for evaluating power semiconductors. In Proceedings of the 2018 IEEE Applied Power Electronics Conference and Exposition (APEC), San Antonio, TX, USA, 4–8 March 2018; pp. 2861–2867.
3. Lu, J.L.; Hou, R.; Chen, D. Opportunities and design considerations of GaN HEMTs in ZVS applications. In Proceedings of the 2018 IEEE Applied Power Electronics Conference and Exposition (APEC), San Antonio, TX, USA, 4–8 March 2018; pp. 880–885.
4. Liu, J.; Xia, C.; Liu, L.; Wang, X. Matrix Extraction of Parasitic Parameters and Suppression of Common-Mode Conducted Interference in a PMSG-IDOS Rectifier Module. *Electronics* **2020**, *9*, 206. [\[CrossRef\]](#)
5. Arnold, M.; Laird, I.D.; Longford, A.; Yuan, X. Experimental evaluation of a low-cost QFN silicon carbide half-bridge module. *IEEE Trans. Compon. Packag. Manuf. Technol.* **2019**, *9*, 1603–1612. [\[CrossRef\]](#)
6. Su, G.-J.; White, C.; Liang, Z. Design and evaluation of a 6.6 kW GaN converter for onboard charger applications. In Proceedings of the 2017 IEEE 18th Workshop on Control and Modeling for Power Electronics (COMPEL), Stanford, CA, USA, 9–12 July 2017; pp. 1–6.
7. Ramachandran, R.; Nymand, M.; Petersen, N.H. Design of a compact, ultra high efficient isolated DC-DC converter utilizing GaN devices. In Proceedings of the IECON 2014—40th Annual Conference of the IEEE Industrial Electronics Society, Dallas, TX, USA, 29 October–1 November 2014; pp. 4256–4261.
8. Ramachandran, R.; Nymand, M. Analysis of capacitive losses in GaN devices for an isolated full bridge DC-DC converter. In Proceedings of the 2015 IEEE 11th International Conference on Power Electronics and Drive Systems, Sydney, NSW, Australia, 9–12 June 2015; pp. 467–472.
9. Ramachandran, R.; Nymand, M. Design and analysis of an ultra-high efficiency phase shifted full bridge GaN converter. In Proceedings of the 2015 IEEE Applied Power Electronics Conference and Exposition (APEC), Charlotte, NC, USA, 15–19 March 2015; pp. 2011–2016.
10. Cioni, M.; Bertacchini, A.; Mucci, A.; Zagni, N.; Verzellesi, G.; Pavan, P.; Chini, A. Evaluation of V_{TH} and R_{ON} Drifts during Switch-Mode Operation in Packaged SiC MOSFETs. *Electronics* **2021**, *10*, 441. [\[CrossRef\]](#)
11. Song, S.; Hu, Y.; Ni, K.; Yan, J.; Chen, G.; Wen, H.; Ye, X. Multi-port high voltage gain modular power converter for offshore wind farms. *Sustainability* **2018**, *10*, 2176. [\[CrossRef\]](#)
12. Qiu, Y.; Liu, W.; Fang, P.; Liu, Y.-F.; Sen, P.C. A mathematical guideline for designing an AC-DC LLC converter with PFC. In Proceedings of the 2018 IEEE Applied Power Electronics Conference and Exposition (APEC), San Antonio, TX, USA, 4–8 March 2018; pp. 2001–2008.
13. Roccaforte, F.; Fiorenza, P.; Greco, G.; Nigro, R.L.; Giannazzo, F.; Iucolano, F.; Saggio, M. Emerging trends in wide band gap semiconductors (SiC and GaN) technology for power devices. *Microelectron. Eng.* **2018**, *187–188*, 66–77. [\[CrossRef\]](#)
14. Stecca, M.; Abdelhakim, A.; Soeiro, T.B.; Canales, F.; Bauer, P.; Palensky, P. Hybrid Space Vector Modulation Scheme for the Multiport Hybrid Converter. *IEEE Trans. Power Electron.* **2022**, *38*, 60–65. [\[CrossRef\]](#)
15. Almutairi, A.; Sayed, K.; Albagami, N.; Abo-Khalil, A.G.; Saleeb, H. Multi-port PWM DC-DC power converter for renewable energy applications. *Energies* **2021**, *14*, 3490. [\[CrossRef\]](#)
16. Savrun, M.M.; İnci, M.; Büyük, M. Design and analysis of a high energy efficient multi-port dc-dc converter interface for fuel cell/battery electric vehicle-to-home (V2H) system. *J. Energy Storage* **2022**, *45*, 103755. [\[CrossRef\]](#)
17. Gevorgov, L.; Domínguez-García, J.L.; Martínez, Á.F. Modern Trends in MultiPort Converters: Isolated, Non-Isolated, and Partially Isolated. In Proceedings of the 2022 IEEE 63th International Scientific Conference on Power and Electrical Engineering of Riga Technical University (RTUCON), Riga, Latvia, 10–12 October 2022; pp. 1–6.
18. Reddi, N.K.; Ramteke, M.R.; Suryawanshi, H. Design and Realization of Current-Fed Single-Input Dual-Output Soft-Switched Resonant Converter. *J. Circuits Syst. Comput.* **2020**, *29*, 2050069. [\[CrossRef\]](#)
19. Li, H.; Bai, L.; Zhang, Z.; Wang, S.; Tang, J.; Ren, X.; Li, J. A 6.6 kW SiC bidirectional on-board charger. In Proceedings of the 2018 IEEE Applied Power Electronics Conference and Exposition (APEC), San Antonio, TX, USA, 4–8 March 2018; pp. 1171–1178.
20. Yi, W.; Ma, H.; Peng, S.; Liu, D.; Ali, Z.M.; Dampage, U.; Hajjiah, A. Analysis and implementation of multi-port bidirectional converter for hybrid energy systems. *Energy Rep.* **2022**, *8*, 1538–1549. [\[CrossRef\]](#)
21. Jayaram, N.; Halder, S.; Panda, K.P.; Pulavarthi, S.V.K. A Novel Design With Condensed Component of Multi-Input High Gain Nonisolated DC-DC Converter for Performance Enhancement in Carbon Neutral Energy Application. *IEEE J. Emerg. Sel. Top. Ind. Electron.* **2022**, *4*, 37–49.
22. Shoaie, A.; Abbaszadeh, K.; Allahyari, H. A Single-Inductor Multi-Input Multilevel High Step-Up DC-DC Converter Based on Switched-Diode-Capacitor Cells for PV Applications. *IEEE J. Emerg. Sel. Top. Ind. Electron.* **2022**, *4*, 18–27. [\[CrossRef\]](#)

23. Lai, C.; Shyu, K. A single-stage AC/DC converter based on zero voltage switching LLC resonant topology. *IET Electr. Power Appl.* **2007**, *1*, 743–752. [[CrossRef](#)]
24. Do, H.-L.; Kwon, B.-H. Single-stage asymmetrical PWM AC–DC converter with high power factor. *IEE Proc. Electr. Power Appl.* **2002**, *149*, 1–8. [[CrossRef](#)]
25. Faizan, M.; Bi, J.; Liu, M.; Wang, L.; Stempitsky, V.; Yousaf, M.Z. Long Life Power Factor Corrected LED Driver with Capacitive Energy Mechanism for Street Light Applications. *Sustainability* **2023**, *15*, 3991. [[CrossRef](#)]
26. O’Sullivan, D.L.; Egan, M.G.; Willers, M.J. A family of single-stage resonant AC/DC converters with PFC. *IEEE Trans. Power Electron.* **2009**, *24*, 398–408. [[CrossRef](#)]
27. Li, H.; Zhang, Z.; Wang, S.; Tang, J.; Ren, X.; Chen, Q. A 300-kHz 6.6-kW SiC bidirectional LLC onboard charger. *IEEE Trans. Ind. Electron.* **2019**, *67*, 1435–1445. [[CrossRef](#)]
28. Gupta, P.P.; Kumar, N.; Nangia, U. Design and Analysis of LLC Resonant Converter and CCCV Topology for Battery Charging. In Proceedings of the 2022 2nd Asian Conference on Innovation in Technology (ASIANCON), Ravet, India, 26–28 August 2022; pp. 1–5.
29. Santra, S.B.; Roy, A.; Choudhury, T.R.; Chatterjee, D.; Nayak, B. Performance improvement of DC-DC converter using L-D-based modified GaN-FET driver. *Int. J. Circuit Theory Appl.* **2020**, *48*, 860–873. [[CrossRef](#)]
30. Maso, P.; Xu, J.Z. *Why GaN E-HEMTs are a Power Designer’s Transistor of Choice*; GaN Systems, Inc.: Ottawa, ON, Canada, 2019.
31. Systems, G. GS66508B (650V Enhancement Mode GaN Transistor). Available online: <https://gansystems.com/gan-transistors/gs66508b/> (accessed on 13 June 2023).
32. Baliga, B.J. *Fundamentals of Power Semiconductor Devices*; Springer Science & Business Media: New York, NY, USA, 2010.

Disclaimer/Publisher’s Note: The statements, opinions and data contained in all publications are solely those of the individual author(s) and contributor(s) and not of MDPI and/or the editor(s). MDPI and/or the editor(s) disclaim responsibility for any injury to people or property resulting from any ideas, methods, instructions or products referred to in the content.